Journal of Catalysis **181,** 244–255 (1999)
Article ID jcat.1998.2314, available online at http://www.idealibrary.com on IDEAL®

Influence of Cesium in Pt/NaCsβ on the Physico-Chemical and Catalytic Properties of the Pt Clusters in the Aromatization of *n*-Hexane

T. Bécue,* F. J. Maldonado-Hodar,* A. P. Antunes,* J. M. Silva,* M. F. Ribeiro,* P. Massiani,† and M. Kermarec†,[1]

*Departamento de Enghenaria Quimica, Instituto Superior Técnico, Av. Rovisco Pais, 1096 Lisboa, Portugal;
†Laboratoire de Réactivite de Surface, Université P. et M. Curie, 4 place Jussieu, 75252 Paris cedex 05
Fax: 33-01-44-27-60-33, E-mail: Kermarec.ccr.jussieu.fr

Received June 22, 1998; revised October 20, 1998; accepted October 25, 1998

Various Pt/NaCsβ catalysts with decreasing Na/Cs ratios and a Pt/KL sample taken as a reference catalyst for aromatization of *n*-hexane, have been prepared by exchange of NaCsβ and KL zeolites in a Pt tetraammine solution then calcination and reduction. The increase of the Cs content in the NaCsβ zeolitic support results in a decrease of the cyclohexane adsorption and Pt exchange capacities. The Pt/Csβ and Pt/KL samples show similar behaviors which strongly differ from those of the Na-containing Pt/NaCsβ samples in terms of (i) reducibility of the Pt ions after calcination, (ii) shape of the FTIR spectra of CO adsorbed on the Pt clusters after reduction, and (iii) catalytic activity of these clusters in the conversion of *n*-hexane. In particular, the selectivity to aromatization is much higher on the Pt/Csβ and Pt/KL catalysts than on the Na-containing Pt/NaCsβ ones. The reasons for the specific behaviors of the Pt/Csβ and Pt/KL samples are discussed. © 1999 Academic Press

Key Words: **Csβ zeolite; Pt clusters; aromatization; TPR; FTIR of adsorbed CO.**

INTRODUCTION

Much attention has been paid in the past 15 years to the three-dimensional large-pore β zeolite because of its remarkable behavior as an acid catalyst for the transformation of petrochemicals (1), fine chemicals (2), and organic compounds (3). The remarkable acid properties of this zeolite have been assigned to the presence of numerous local defects (4) in its highly faulted crystalline structure which consists in the intergrowth of two polymorphs (tetragonal and monoclinic) (5). The β structure is also highly flexible, allowing strong variations in the T-O-T angles which may be at the origin of the basic behavior of this zeolite (6, 7) in spite of its low Al content (Si/Al > 12) usually associated to an average Sanderson's electronegativity typical of nonbasic materials (8). On the one hand, the basic sites in alkali (Na, Cs) exchanged β samples have been evidenced by the downward FTIR shift of the NH band of adsorbed pyrrole (9, 10). On the other hand, they have been revealed by the basic catalytic behavior of sodium β catalysts in the Knoevenagel condensation of benzaldhehyde with esters (6).

Since the initial report of Bernard on the noteworthy aromatization properties of platinum clusters supported on nonacidic zeolites (11) many investigations have been undertaken on the characterization of Pt supported on basic zeolites or oxides. Many attempts have been made to explain the remarkable catalytic behavior of the Pt/KL system towards aromatization, but the reasons for it still remain a matter of debate. The optimization of this catalyst has been performed by introducing alkali-earth or alkali cations at appropriate steps of the preparation to minimize the acidity (12, 13). Besides, the choice of the Pt precursor and the mode of its deposition followed by a suitable calcination treatment have been thoroughly studied (11, 14–16). The main hypotheses which have been proposed to explain the properties of the Pt clusters on basic supports are (i) the role of the basicity of the support and of the metal–support interactions (17, 18), (ii) the infuence of the geometry of the channels leading to the concepts of the molecular die (19, 20) and of the structural recognition and preorganisation of the alkane molecule (21), and (iii) the platinum cluster size (13, 22). The available physicochemical and catalytic data on these factors have recently been reviewed (23, 24).

In spite of the basic character of the alkali-exchanged β zeolite and of its potential interest as a support for platinum, few reports have been devoted to the Pt/alkali-β system for the conversion of *n*-hexane (25, 26). Recently, Pt/Kβ and Pt/BaKβ catalysts were shown to be active in this reaction and their catalytic behavior was found to depend on the conditions of pretreatement (oxidation, reduction) of the catalyst (26a). Moreover, the catalytic performances of acidic Pt/β zeolites were investigated and it was shown that decreasing the acidity of the β support by exchange with Cs^+ cations could enhance the selectivity to benzene (26b). The Pt/Kβ catalysts were more sulfur resistant than the Pt/KL

[1] Corresponding author. E-mail: kermarec@ccr.jussieu.fr.

0021-9517/99 $30.00

ones (26b). Furthermore, we have shown that cesium gives unique properties to the Pt/β system in comparison to the other alkali cations (27).

These features have encouraged us to investigate the influence of the cesium content on the physicochemical properties and on the catalytic behavior of Pt clusters supported on basic NaCsβ in the conversion of *n*-hexane. Therefore, Pt/NaCsβ catalysts with different Na/Cs atomic ratios were prepared and their characterization by several techniques was performed. The results were compared to those obtained on a Pt/KL system taken as a reference. The reduction of platinum precursors was characterized by temperature- programmed reduction (TPR) and the size of the reduced particles determined by transmission electron microscopy (TEM). The electronic and/or geometric effects affecting the platinum particles were probed by FTIR of adsorbed CO. Finally, the catalytic activity of the solids was tested in the conversion of *n*-hexane. These investigations constitute an attempt to understand the role of the different above-mentioned factors in the catalytic efficiency of the samples.

EXPERIMENTAL SECTION

1. Materials

Zeolitic Supports

The parent organic-free β zeolite was supplied by Exxon Chemical Europe (Belgium) in a partially protonic form (HNaβ). This material was exchanged twice with a 0.5 *M* $NaNO_3$ solution in order to ensure a complete exchange of the protons. The ion exchange was carried out during 2 h under vigorous stirring at 80°C, using a ratio "volume of solution (mL)/weight of zeolite (g)" of 70. The sodium exchanged solid (sample Naβ) was recovered after centrifugation and washed with deionized water. Partially (samples $Na_{75}Cs_{25}\beta$, $Na_{60}Cs_{40}\beta$, and $Na_{25}Cs_{75}\beta$) and totally (sample Csβ) cesium-exchanged samples were obtained as follows: four portions (2 g each) of the sodium form zeolite (Naβ) were exchanged during 2 h under stirring at 80°C in 140 ml of $CsCH_3COO$ solutions with increasing concentrations (3×10^{-3}, 6×10^{-3}, 9×10^{-3}, and 0.5 *M*). The exchange with the 0.5 *M* solution was repeated twice in order to ensure a complete exchange of Na by Cs ions. After recovering by centrifugation, washing, and drying overnight at 100°C, the samples were calcined in flowing dried air (3 L/h · g) at 500°C for 2 h. The KL zeolite was a commercial sample from UOP (United States).

Pt-Loaded Zeolites

The KL and sodium and/or cesium-exchanged NaCsβ supports were ion exchanged with $Pt(NH_3)_4^{2+}$ by contacting 1 g of each sample with a 5×10^{-4} *M* aqueous solution of $Pt(NH_3)_4(NO_3)_2$ during 4 h at room temperature under stirring. The expected platinum loading was 0.5 wt%. The Pt loaded zeolites (samples Pt/NaCsβ and Pt/KL) were subsequently filtered, washed with distilled water, and dried for 12 h at 100°C. The catalysts were then calcined in a pyrex reactor in flowing dried air (3 L/h · g) up to 300°C (heating rate of 2°C/min) and maintained at this temperature for 2 h. After calcination, the samples (called below "calcined samples") were cooled down to room temperature, purged with helium, and kept in a dessicator at room temperature before characterization.

2. Techniques of Characterization

Physicochemical Characterizations

The X-ray diffraction (XRD) patterns were recorded on a Siemens D500 automatic diffractometer with a Cu K_α monochromatized radiation source. Structural bands of the NaCsβ supports were characterized by using KBr pellets (0.5 mg of zeolite in 200 mg of KBr) on a Bruker IFS 66 V Fourier-transform spectrometer.

Dynamic adsorption of cyclohexane was carried out on the NaCsβ and KL supports using a Setaram TG-DSC92 thermobalance. After pretreatment under N_2 at 500°C (2°C/min) for 10 min, the samples were cooled down to 90°C. Once the sample weight stabilized, the N_2 flow was switched to a N_2-cyclohexane flow obtained by bubbling N_2 (50 mL/min) in a cyclohexane saturator at 14.6°C and the weight increase was measured as a function of time.

Elemental analysis of the solids before and after Pt loading was obtained by atomic absorption from the Service Central d'Analyse du Centre National de Recherche Scientifique (Vernaison, France).

$Pt(NH_3)_4^{2+}$ Decomposition and Reduction

The decomposition of the tetraammine platinum complex in oxygen (TPO, 5% O_2 in He, 5 mL/min) or in helium (TPHe, 5 mL/min) was studied by mass spectrometry (MS) using a Quadruvac PGA 100 mass spectrometer. The experiments were conducted at a heating rate of 5°C/min from room temperature to 900°C and 70 mg of sample were used for each run.

Prior to TPR experiments, the calcined Pt/NaCsβ and Pt/KL samples (100–200 mg) were heated at 200°C for 1 h in argon (25 mL/min) and subsequently cooled down to room temperature. The Ar flow was then switched to a 5% H_2/Ar mixture flowing at the same rate. For the TPR experiments, the temperature was ramped at a rate of 10°C/min up to 800°C while the H_2 consumption was monitored by a TCD detector.

Characterization of the Metal Particles

TEM images of the platinum particles were obtained on a Jeol 100CXII microscope. The calcined zeolites were

reduced in flowing hydrogen (3 L/h · g, 2°C/min) up to a temperature of 200°C for 2 h, then at 500°C for 5 h. Histograms of the metal particle size distributions were established by counting about 1000 particles. The mean particle diameter was calculated by using the formula $d_m = \sum n_i d_i / n_i$, where n_i is the number of particles of diameter d_i.

Transmission FTIR spectra of CO adsorbed on the supported platinum clusters were collected at a resolution of 4 cm^{-1} and after accumulation of 128 scans using a Bruker IFS 66 V Fourier-transform spectrometer. Self-supported wafers (ca 20 mg, 18 mm in diameter, pressed under a pressure of 10^3 kg · cm^{-2}) of calcined Pt/NaCsβ and Pt/KL samples were placed on a quartz holder which was introduced into an infrared cell equipped with KBr windows and connected to a classical vacuum line. The wafers were *in-situ* reduced in flowing hydrogen at 500°C for 5 h, then outgassed ($P < 5 \times 10^{-5}$ mbar) for one hour at this temperature and cooled down to room temperature. The background spectrum was that of the sample after reduction. Carbon monoxide was first adsorbed at a pressure of 5×10^{-2} mbar at room temperature (RT) for 15 min. In order to achieve a good distribution of the CO molecules on all the metal particles and to minimize the dipole–dipole interactions, the samples were then heated in the presence of this residual CO pressure at 100°C for 1 h, and subsequently outgassed at that temperature for 1 h ($P < 10^{-5}$ mbar). After this treatment, the dipole–dipole contribution strongly decreased. An outgassing treatment at 150°C for 15 h led to an almost complete disappearance of the CO bands. It was also checked that the unloaded supports did not give rise to a CO adsorption signal. Peak positions were determined by the Bruker Fit curve procedure.

Catalytic Tests

The *n*-hexane conversion reaction was performed in a flow reactor, at 450°C under a total pressure of 1 bar. The calcined Pt/NaCsβ and Pt/KL catalysts were *in-situ* reduced by flowing hydrogen at 500°C for 5 h. The reaction feed consisted in a mixture of hydrogen and *n*-hexane (molar ratio of 6 to 1) which was homogeneized in a preheated (80°C) vaporizator. The space velocity (WHSV) varied from 15 to 45 h^{-1}, H_2 being used as a carrier gas. The reaction products were separated and identified by an on-line Hewlett–Packard chromatograph, equipped with a 50 m plot capillary column (PONA) and a flame ionization detector (FID). Results are reported as conversions (percentage of *n*-hexane moles reacted) and product selectivities (weight of product divided by weight of *n*-hexane reacted, in percent).

RESULTS

1. Chemical and Textural Characterizations

Zeolitic Supports

The unit-cell compositions of the KL and NaCsβ zeolites, deduced from atomic absorption analysis of Si, Al, Na, and Cs, are reported in Table 1. The results confirm that the compensating cations in the β zeolite are easily exchangeable. This table also reports the average charge on the oxygen atoms of the Pt-free zeolites, calculated using the Sanderson equalization principle of electronegativities (8). It is noteworthy that the average charge on the oxygen atoms of the β zeolite lattice does not change to a large extent by varying the cesium amount, due to the high Si/Al ratio (low number of countercations).

The crystallinity of the β zeolite after Na and/or Cs exchange was checked by FTIR spectroscopy and X-ray diffraction (spectra not shown for the sake of brevity). For all the NaCsβ samples, the FTIR bands in the wavenumber range 700–400 cm^{-1}, associated with skeletal modes characteristic of highly crystalline β (28), are retained. Moreover, the XRD patterns are charateristic of the β structure. The lower intensity of the diffraction peaks when the Cs content increases results mostly from a higher X-ray absorption coefficient of cesium. A small loss of crystallinity of the NaCsβ samples after calcination, estimated from the

TABLE 1

Chemical Composition of the Samples before and after Pt Loading

Before Pt loading							After Pt loading						
	Atoms per unit-cell[a]								Atoms per unit cell[a]				
Supports	Na	Cs	K	Al	Si	δ_O[b]	Catalysts	Pt (wt%)	Pt	Na	Cs	K	Al	Si
Naβ	3.6	—	—	4.0	60.0	−0.313	Pt/Naβ	0.58	0.13	3.7	—	—	4.0	60.0
$Na_{75}Cs_{25}\beta$	2.6	0.9	—	4.0	60.0	−0.314	$Pt/Na_{75}Cs_{25}\beta$	0.53	0.12	2.7	0.9	—	4.0	60.0
$Na_{60}Cs_{40}\beta$	2.4	1.4	—	4.0	60.0	−0.315	$Pt/Na_{60}Cs_{40}\beta$	0.48	0.11	2.3	1.2	—	4.0	60.0
$Na_{25}Cs_{75}\beta$	0.9	3.0	—	4.0	60.0	−0.317	$Pt/Na_{25}Cs_{75}\beta$	0.43	0.10	0.8	3.0	—	4.0	60.0
Csβ	—	3.5	—	4.1	59.9	−0.318	Pt/Csβ	0.27	0.06	—	3.9	—	4.1	59.9
KL	—	—	8.9	9.0	27.0	−0.391	Pt/KL	0.35	0.05	—	—	8.8	9.0	27.0

[a] Unit cell of 64 and 36 tetrahedra (Si, Al atoms) for the β and L structures, respectively.
[b] Average Charge on the Lattice Oxygens on the Zeolitic Supports.

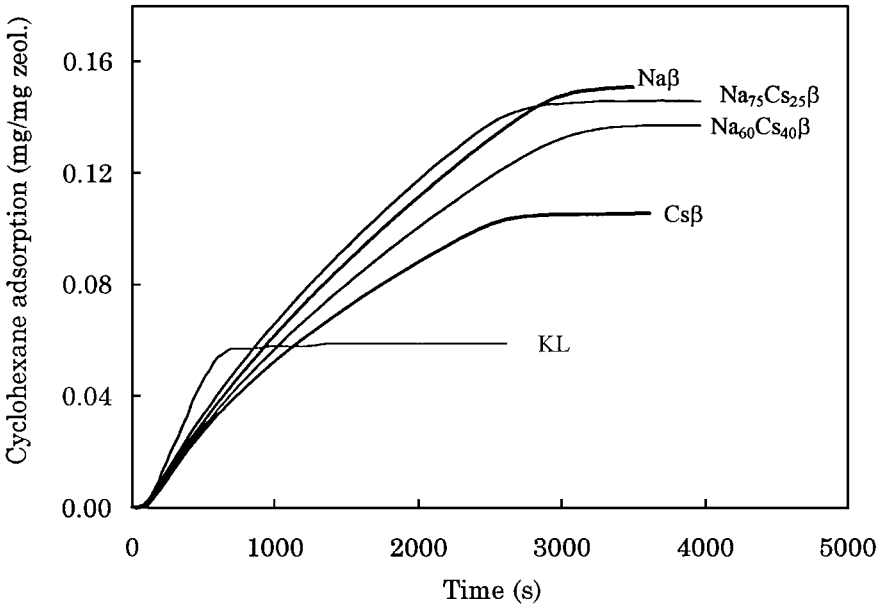

FIG. 1. Dynamic adsorption of cyclohexane in the NaCsβ and KL zeolitic supports.

area of the most intense peak at $2\theta = 22.5°$, corrected from the X-ray absorption changes due to the different Na/Cs ratios (29), was observed. The values obtained indicate that the NaCsβ catalysts remain highly crystalline since only the Csβ catalyst loses around 7% of crystallinity.

Figure 1 compares the dynamic adsorption of cyclohexane in the various NaCsβ and KL zeolitic supports. In spite of an initial rate of adsorption larger for KL than for the NaCsβ samples, the adsorption capacity is significantly smaller in KL, in agreement with the smaller pore volume of this unidirectionel microporous structure. For comparison, the micropore volumes classically reported for β (30) and L (31) zeolites are around 0.25 and 0.16 mL/g, respectively. Besides, the amount of cyclohexane adsorbed at equilibrium decreases proportionnally to the cesium content as illustrated on Fig. 2. It is noteworthy that the adsorption capacity of the NaCsβ supports tends to that of the KL zeolite with increasing cesium loading.

Pt Loaded Zeolites

The NaCsβ and KL zeolitic supports were exchanged by platinum tetraammine in identical conditions, corresponding to the same expected amount of platinum (0.5 wt% corresponding to 0.12 Pt atoms per unit cell). In spite of these constant experimental conditions, the Pt loading in KL is about 30% lower than that in Naβ (Table 1). Moreover, in the NaCsβ series, it decreases when the Cs/Na atomic ratio increases and the decrease is proportional to the increase of the cesium content as already observed for the cyclohexane adsorption capacity (Fig. 2). It is unlikely that the lowering of the cyclohexane adsorption and of the Pt exchange capacities when increasing the Cs/Na ratio in β are related to a partial collapse of the zeolite framework since the XRD patterns, and the FTIR structural bands of NaCsβ samples show that the samples remain highly crystalline. This lowering rather suggests a partial blockage of the β porosity by the bulky cesium cations.

Besides, no peaks characteristic of a Pt metallic phase are detected by XRD after reduction of the catalyst samples. This was expected in view of the weak Pt loading and it confirms that the Pt particles are small. Furthermore, no FTIR bands of framework-bridged hydroxyls (Brönsted acid sites) at 3610 cm^{-1} are detected in the reduced Pt samples (spectra not shown), suggesting that the amount of

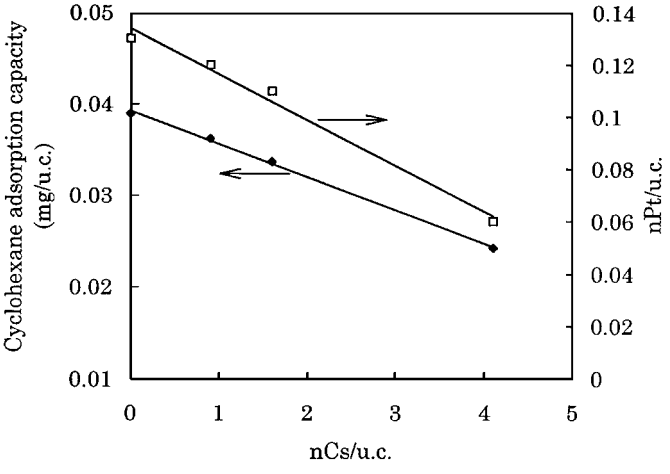

FIG. 2. Capacity of cyclohexane adsorption and number of exchanged Pt atoms per unit cell as a function of the number of Cs atoms per unit cell in the NaCsβ zeolites.

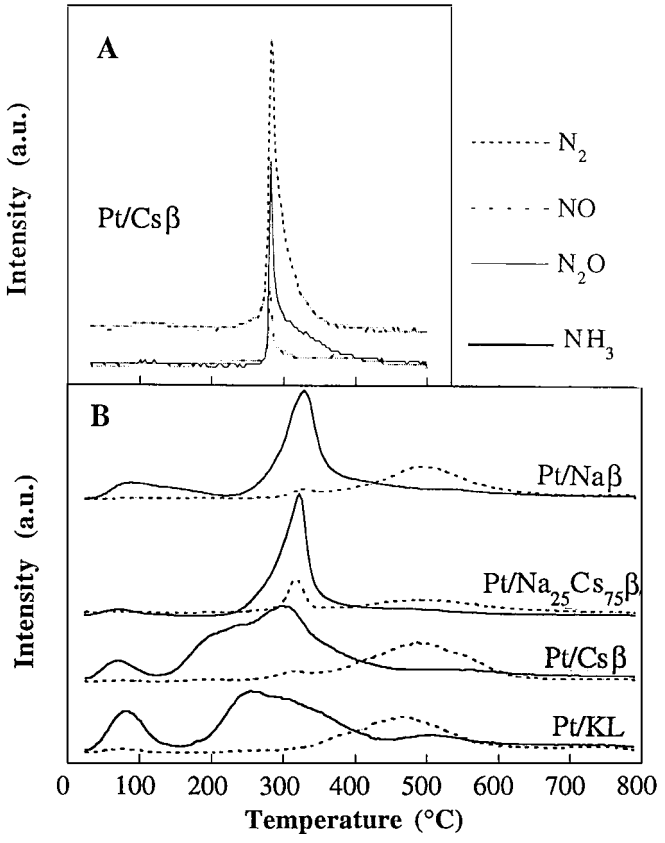

FIG. 3. Evolution of NH_3 (mass 17), N_2 (mass 28), N_2O (mass 44), and NO (mass 30) during decomposition upon heating (5°C/min) in (A) oxygen (5 mL/min 5% O_2/He) or in (B) He (5 mL/min He) of the $Pt(NH_3)_4^{2+}$ complex exchanged in the NaCsβ and KL zeolites. The TPO curves in (A) are identical whatever the zeolitic support.

protons produced by reduction of the platinum ions is too small to be detectable in the FTIR spectra of the β samples.

2. Decomposition of the Platinum Tetraammine Precursor

The thermal decomposition in oxygen (TPO) or in helium (TPHe) of the ammonium ligands of the exchanged Pt tetraammine complexes is revealed by the evolution of NH_3 (masses 14 to 17), N_2 (masses 14 and 28), N_2O (masses 30 and 44), and NO (masses 14, 16, and 30).

When the decomposition is performed in oxygen (TPO), the MS spectra are identical, regardless of the zeolite support. A typical spectrum is reported in Fig. 3A. The zeolite is dehydrated below 200°C (mass 18, not shown) and the ammine ligands are subsequently decomposed in the temperature range 200–300°C as revealed by the evolution of N_2, N_2O, and NO. The decomposition in oxygen of the ammine complexes in alkali β zeolite is achieved below 300°C.

The decomposition in helium (TPHe) contrasts with the above observations and some differences are observed from one sample to another (Fig. 3B). The process of the Pt tetraammine decomposition is similar for the Na-containing NaCsβ supports as shown by the curves reported for the Naβ and $Na_{25}Cs_{75}\beta$ ones, the ammine ligands being first released as NH_3 (with some N_2) around 320°C, then as N_2 around 500°C. The process is significantly different for the Pt/Csβ and Pt/KL samples for which the evolution of NH_3 occurs at a temperature lower than above and in at least two steps centered around 200 and 300°C. It is well known that autoreduction occurs during the decomposition of metal tetraammine complexes in helium, leading to large particles with no practical interest for catalysis. However, the similarity of the behaviors of the Pt/KL and the Pt/Csβ compounds, as far the NH_3 removal is concerned must be emphasized.

3. Platinum Reducibility and Particle Size

The TPR profiles of the calcined Pt/NaCsβ and Pt/KL samples are compared in Fig. 4. For the sake of clarity, the curves for the intermediate $Pt/Na_{40}Cs_{60}\beta$ and $Pt/Na_{75}Cs_{25}\beta$ (close to that of $Pt/Na_{25}Cs_{75}\beta$) are not reported. The TPR profiles of Pt/Naβ and Pt/Csβ markedly differ. Thus, a single sharp peak around 400°C is observed for the Pt/Naβ sample, whereas two peaks centered around 230°C and 450°C (with a shoulder around 400°C) are found for Pt/Csβ. Moreover, the quantitative analysis of the curves indicate that the consumption of H_2 corresponds to a H/Pt ratio of 1.9 for the Pt/Naβ sample, whereas it equals 7 for the Pt/Csβ zeolite. In the case of the intermediate Pt/NaCsβ samples, the peak around 400°C is the only one identified but it is significantly broader (380–520°C) than that observed for the Pt/Naβ zeolite. It may be underlined that the Pt/KL zeolite also exhibits two peaks, corresponding to a high consumption of H_2 (H/Pt = 9), with maxima at temperatures around 230 and 420°C, close to those observed for the Pt/Csβ sample.

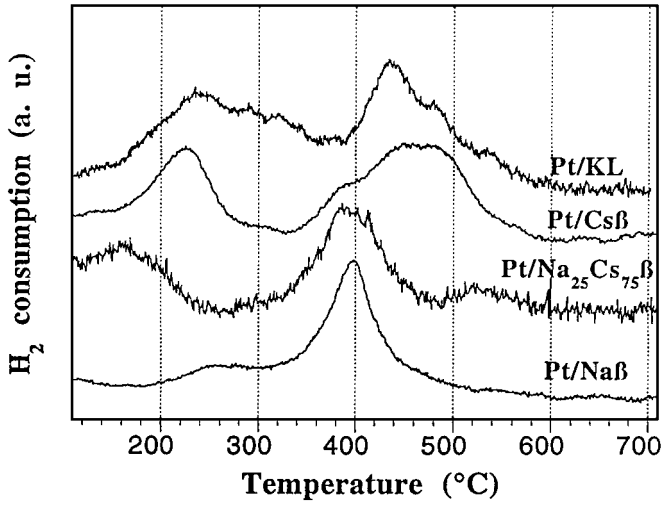

FIG. 4. TPR profiles (25 mL/min 5% H_2/Ar, 10°C/min) of Pt/NaCsβ and Pt/KL samples previously calcined at 300°C.

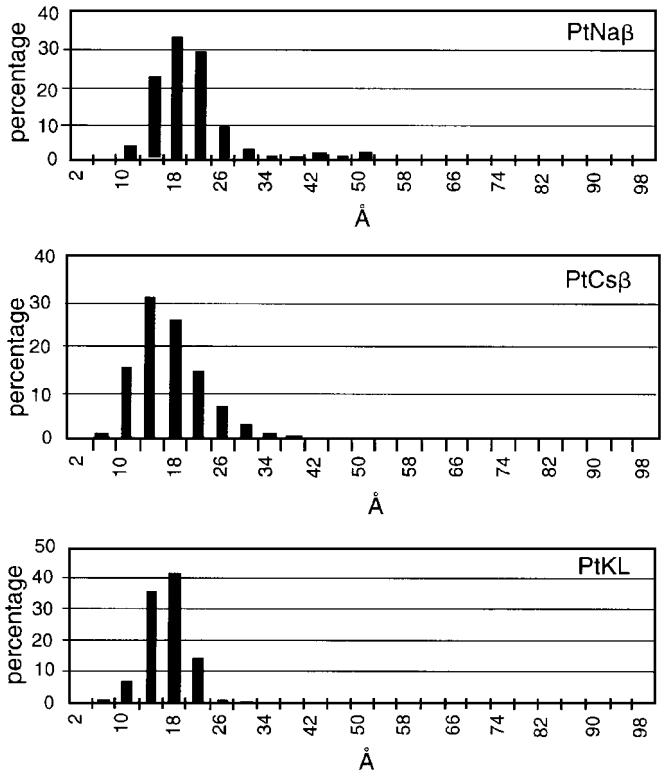

FIG. 5. Distribution of the platinum particle sizes (expressed as a number of particles percentage) in the reduced Pt/Naβ, Pt/Csβ, and Pt/KL samples.

TEM images of the Pt/Naβ, Pt/Csβ, and Pt/KL zeolites were taken after reduction of the solids at 500°C. The size distribution of the metal particles visible in the micrographs are reported in Fig. 5. The narrowest distributions are observed for the Pt/KL and Pt/Csβ samples with a mean diameter d_m of about 17 Å. Unfortunately, this evaluation cannot take into account the very small particles possibly present but not detectable by TEM (Pt particles with a diameter lower than 7 Å are not detected by our microscope). For the Pt/Naβ sample, some scarce but large particles ($40 < d < 180$ Å) are also observed (particles with $d > 100$ Å not seen in Fig. 5). These particles are obviously located at the external surface of the zeolite but their amount is negligible, in comparison with the total number of particles. The presence of these large particles suggests that some autoreduction occured during calcination in air (32) which is indeed confirmed since the calcined Pt/Naβ sample already exhibits Pt particles before reduction (histogram not given).

4. Catalytic Results

The catalytic results in the *n*-hexane transformation of the Pt/NaCsβ and Pt/KL catalysts are reported in Tables 2 and 3 and in Figure 6. Table 2 gives the conversions of *n*-hexane and selectivities to the main products of reaction (aromatization, isomerization, and cracking) for the Pt/NaCsβ and Pt/KL catalysts for the "fresh" and "used" catalysts (corresponding to 0.1 and 2 *h* of time on stream, respectively). Figure 6 plots the selectivities to benzene obtained during the runs as a function of conversions. Due to higher activities of the Na-containing Pt/NaCsβ catalysts, as compared to the Pt/Csβ and Pt/KL ones (Table 2), the WHSV were modified by varying the contact times in order to allow the comparison of selectivities in ranges of close conversions. The conversions are in the range 25–70% for the Na-containing Pt/NaCsβ samples and in the range

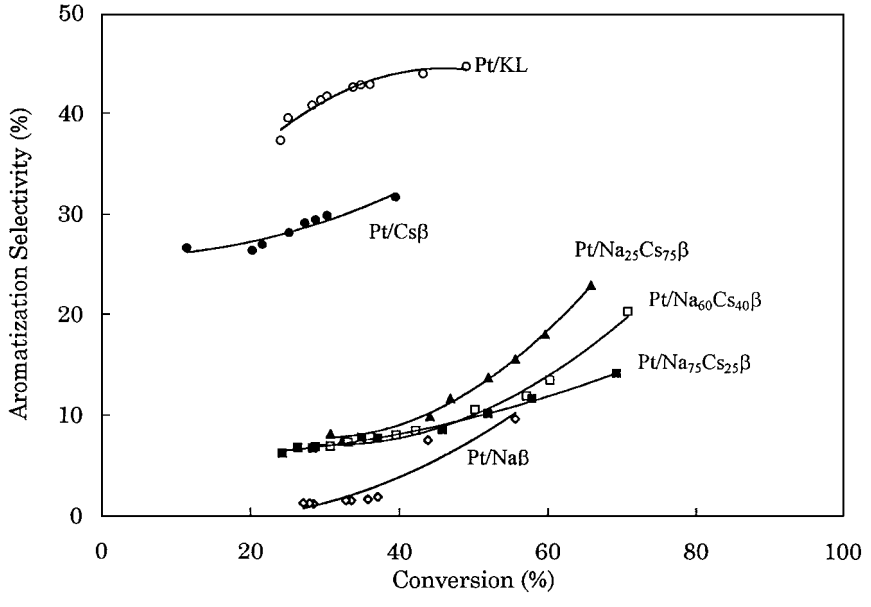

FIG. 6. Selectivity to benzene as a function of n-hexane conversion on the Pt/NaCsβ and Pt/KL catalysts.

TABLE 2

Conversion, Product Selectivity, and Coefficient of Deactivation during *n*-Hexane Transformation Reactions at 723 K on the Pt/NaCsβ and Pt/KL Catalysts

Samples	WHSV (h^{-1})	Conversion (%)	Product selectivity			$D_{benzene}$[c] (%)
			Benzene (wt%)	Isomers (wt%)	Cracking (wt%)	
Pt/Naβ						
fresh[a]	45	56	10	72	18	
used[b]		28	1	93	6	95
Pt/$Na_{75}Cs_{25}\beta$						
fresh[a]	35	69	14	61	25	
used[b]		26	7	85	8	80
Pt/$Na_{60}Cs_{40}\beta$						
fresh[a]	25	70	20	50	30	
used[b]		31	7	83	10	84
Pt/$Na_{25}Cs_{75}\beta$						
fresh[a]	15	66	23	52	25	
used[b]		32	8	82	10	83
Pt/Csβ						
fresh[a]	15	39	32	47	21	
used[b]		20	26	57	17	58
Pt/KL						
fresh[a]	15	49	45	35	21	
used[b]		28	41	41	18	48

[a] Fresh: after 0.1 h time on stream.

[b] Used: after 2 h time on stream.

[c] Coefficient of deactivation towards benzene: $D_{benzene} = (Y_{0.1}-Y_2)/Y_{0.1}$, where $Y_{0.1}$ and Y_2 are the yields of benzene after 0.1 and 2 h of time on stream, respectively.

10–50% for the Pt/Csβ and the Pt/KL samples. Table 3 gives the selectivities at isoconversion (39%).

It can be observed that our reference Pt/KL sample is less efficient (lower stability and selectivity) than the best samples reported in the litterature (11–13). This is probably due to differences in the preparation mode.

For all samples, the conversion and selectivities to aromatization and cracking decrease with time on stream, whereas the selectivity to isomerization increases (Table 2). For the Na-containing catalysts, isomerization is the main reaction and after 2 h the selectivity to isomer compounds is more than 80%, while that to aromatics is less than 10%. By contrast, the selectivity to aromatics always remains in the range 25–45% for the Pt/Csβ and Pt/KL catalysts (Table 2). At isoconversion (39%), the selectivity to aromatization is at least three times higher for the Pt particles supported on the Csβ than on the NaCsβ zeolites, drawing the Pt/Csβ catalyst close to the Pt/KL one (Table 3 and Fig. 6). Moreover, the Pt/Csβ and Pt/KL samples are more stable towards aromatization as shown by the lower coefficients of deactivation $D_{benzene}$ (%) calculated as the ratio $(Y_{0.1}-Y_2)/Y_{0.1}$, where $Y_{0.1}$ and Y_2 are the yields of benzene after 0.1 and 2 h of run, respectively (Table 2).

These catalysts exhibited the same behavior in the transformation of *n*-heptane into toluene as observed for the conversion of *n*-hexane in Fig. 6, with a higher selectivity to toluene for Pt/KL and Pt/Csβ, in comparison to the Na-containing catalysts (figure not shown for the sake of brevity) (63).

TABLE 3

Product Selectivity at Isoconversion (39%) in the *n*-Hexane Transformation Reactions at 723 K on the Pt/NaCsβ and Pt/KL Catalysts

Samples	Product selectivity (wt%)		
	Benzene	Isomers	Cracked molecules
Pt/Naβ	9.9	86.6	3.5
Pt/$Na_{75}Cs_{25}\beta$	7.2	80.0	12.8
Pt/$Na_{60}Cs_{40}\beta$	8.1	80.0	11.9
Pt/$Na_{25}Cs_{75}\beta$	8.0	81.0	11.0
Pt/Csβ	32.0	47.0	21.0
Pt/KL	43.5	37.0	19.5

5. FTIR Study of CO Adsorbed on Pt Particles

The spectra of CO adsorbed on the Pt/NaCsβ compounds are shown in Figs. 7A (adsorption at room temperature) and 7B (subsequent heating at 100°C and outgassing for 1 h at the same temperature). For all samples, the linear

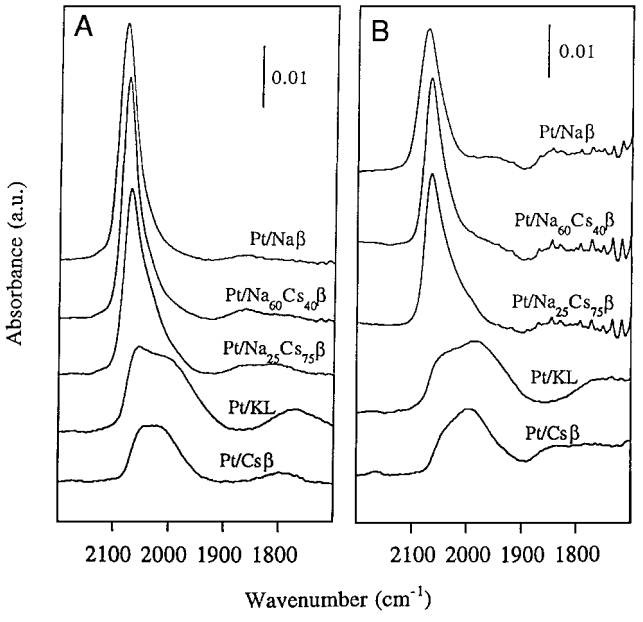

FIG. 7. FTIR spectra of CO adsorbed on the Pt metal particles in Pt/NaCsβ and Pt/KL samples recorded after evacuation (A) at room temperature and (B) at 100°C.

CO species (1900–2150 cm^{-1}) are predominant, the intensities of the bridging CO bands (1750–1900 cm^{-1}) being very low as usually observed for small Pt particles (33). The frequencies of the maxima of the bands of linearly bound CO molecules are reported in Table 4.

For CO adsorbed at room temperature (Fig. 7A), a single and smooth peak is observed for the Na-containing β samples with slight differences in its position (2080–2071 cm^{-1}). A broadening towards the low frequencies appears for the $Pt/Na_{25}Cs_{75}\beta$ sample but the shape of the signal is not significantly modified. In contrast, the spectra of Pt/Csβ is strongly different and resembles that of Pt/KL with the presence of at least two components at much lower frequencies (2043, 1997 and 2057, 1983 cm^{-1} for Pt/Csβ and Pt/KL, respectively).

At 100°C, a decrease in intensity can be noticed for the Na-containing β samples with a shift to lower frequencies due to decreased dipole–dipole coupling interactions (Fig. 7B and Table 4). For the Pt/Csβ and Pt/KL samples, a significant increase of the intensity of the low frequency component is observed at the expense of the high frequency component . One more time, the Pt/Csβ compound shows an analogous behavior with that of the Pt/KL catalyst, with the same CO band shape and with similar wavenumbers of the maxima.

TABLE 4

Frequency of the Maxima of the FTIR Bands of CO Adsorbed on Pt Metal Particles in the Pt/NaCsβ and Pt/KL Catalysts

Samples	ν_{CO} (cm^{-1}) adsorption at RT	ν_{CO} (cm^{-1}) after treatment at 100°C
Pt/Naβ	2080	2062
$Pt/Na_{75}Cs_{25}\beta$	2076	2068
$Pt/Na_{50}Cs_{50}\beta$	2076	2067
$Pt/Na_{25}Cs_{75}\beta$	2071	2065
Pt/Csβ	2030	1997
Pt/KL	2055	1983

DISCUSSION

On the basis of the TPR, TPHe, FTIR, and catalytic data, two sets of samples may be distinguished among the Pt/NaCsβ and Pt/KL zeolites which are, on the one hand, the Na-containing Pt/NaCsβ samples and, on the other hand, the Pt/Csβ and Pt/KL ones. An analogy between the Csβ and KL supports is also found in terms of cyclohexane adsorption and Pt-exchange capacities which are lower than in the Na-containing β samples.

Considering the Pt/KL reference catalyst, a considerable number of investigations have been already carried out and several proposals reported to explain the high aromatization properties of this system in comparison to Pt supported on conventional acidic (silica and alumina) and basic (magnesia) supports. The main factors which are thought to determine the catalytic properties have recently been reviewed (23, 24). Among these factors, one may quote the interaction of Pt with the basic sites of the L zeolite, leading to an increase in the electron density of the metal particles (14, 17, 18, 34). Other hypotheses are the molecular die concept, based on the terminal end-on adsorption of *n*-hexane on the Pt clusters favoring the C_6-ring closure and leading to aromatics (19, 20) and the so-called confinment model which involves the structural recognition and preorganization of the alkane molecule (21). Other studies comparing the aromatization properties of small Pt particles dispersed on KL, on microporous and macroporous silica, and on carbon call into question the confinment and/or collimation models since these supports do not exhibit a peculiar microporous channel system (13). Moreover, recent investigations on Pt supported on Mg(Al)O showing the efficiency of this system outline the importance of the support basicity (22). Finally, the very small sizes of the platinum particles generated in the Pt/KL zeolites (<1 nm) and their stabilization within the channels appear as a determinant factor responsible for their high aromatization efficiency (13, 22, 35–37).

Turning now to our Pt/NaCsβ catalysts, we have to explain the peculiar behavior of the totally Cs-exchanged Pt/Csβ sample, which brings it close to the Pt/KL zeolite. In view of the above literature data we will consider in the discussion hereafter, the possible roles of (i) the electronic effects related to the metal/basic–support interaction (electronic enrichment of the surface of the particle by

polarization or by transfer of electrons from the support to the metal) (38), (ii) the distribution of the size of the platinum particles involving possible electronic effects due to different particles morphologies and different unsaturated Pt sites (geometric effect), and (iii) the location of the alkali in the zeolitic porosity and its vicinity to the platinum particles.

1. Catalytic Behavior and Particle Sizes

For the Na-containing β samples, isomerization is the predominant reaction and a strong deactivation in aromatization and cracking occurs during the catalytic runs. These results cannot be explained by the residual protonic acidity produced by the reduction of platinum since no well-defined OH bands at 3610 cm^{-1} are observed in the FTIR spectra of the reduced catalysts, suggesting a low amount of protons. The catalytic results may rather be understood by considering the size of the platinum particles.

In the Pt/Naβ sample, metal particles with an average diameter $d = 21$ Å are formed, embedded within the zeolite framework. This size, higher than that of the β channels suggests a local destruction of the zeolitic walls. Larger particles ($50 < d < 200$ Å) are also present at the external surface of the zeolite. Such large particles are known to favour isomerization and hydrogenolysis and to contribute to the deactivation (24). In the case of the Pt/Csβ and Pt/KL samples, the Pt particles are slightly smaller, with an average diameter $d = 17$ Å.

A difference in the average particle size of 4 Å is not sufficient to explain the difference in selectivity to aromatization exhibited by our β samples. Moreover, the mean diameter of 17 Å measured for Pt/Csβ is significantly higher than that usually evoked in the literature for the platinum particles in Pt/KL ($d \approx$ or < 10 Å) responsible for increased aromatization and lower deactivation. Thus, very small Pt clusters of 5–6 atoms have been proposed from EXAFS analysis (16, 37, 39). The hypothesis of Pt clusters with $d < 10$ Å is in line with the H/Pt ratios higher than 1 found for hydrogen chemisorption measurements (14, 37). Moreover, TEM images of Pt/KL have shown that the Pt particles are hardly detectable (15, 20a, 40). Therefore, these data lead us to consider the existence of very small particles, not detected by TEM and not included in the calculated average diameter, in our Pt/KL and Pt/Csβ samples which show higher stability and selectivity to aromatization than the Na-containing Pt/NaCsβ catalysts.

In 1979, Bernard *et al.* reported a high selectivity to benzene for Pt/KL samples (1% Pt), exhibiting Pt particles with a mean size around 20 Å (41). Thus, taking into account the more recent hypotheses, it is likely that the high efficiency of those catalysts is due to the presence of small particles not detected by the microscope available at that time.

2. State of Platinum before Reduction

TPR profiles of Pt-supported zeolites strongly depend on the conditions of the sample preparation. They are related to the nature (bare Pt cation or Pt oxide) (42)) and oxidation state (Pt^{2+} or Pt^{4+} ions) (15, 42b, 43) of the platinum atoms present after calcination. They also depend on the metal–support interaction (44).

For the Pt/KL system, various TPR profiles were reported. Three peaks at 11, 80, and 150°C, assigned to the reduction of PtO and of two Pt^{2+} species, respectively, were found for a Pt ion-exchanged sample, whereas a peak at 250°C, assigned to Pt^{4+} ions, was observed for an impregnated sample (15). Recently, two peaks at 120 and 230°C were reported for the reduction of a Pt/KL sample prepared by impregnation (45). The above data suggest that the reduction is achieved below 250°C. This could be in line with the fact that the best dispersion of Pt in Pt/KL (23, 46) and Pt/BaKL (12) is obtained when the reduction in flowing hydrogen is performed around 300°C. However, a high-temperature TPR peak centered around 430°C was also found for Pt/KL (32) and Pt/Kβ (26a), together with a lower temperature peak (range 200–230°C), indicating that temperatures higher than 430°C may be required for complete reduction of the Pt ions. The high-temperature peak was also found for Pt/Hβ (43) . For the β zeolite, the peaks at 195 and 430°C were respectively assigned to Pt^{2+} ions located in the main channels and in hidden sites (26a), the nature of the latter being unknown. These peaks strongly resemble those found for our Pt/KL and Pt/Csβ samples.

Although different Pt locations may exist in our Pt/KL and Pt/Csβ samples (for instance, surface or core of the zeolite particules, location in defect sites), a 220°C difference between the 230°C and 450°C TPR signals cannot be explained in terms of diffusional constraints, since hydrogen molecules diffuse very rapidly. It is likely that these two peaks reveal the contribution of species of a different nature (oxide or bare ions), different oxidation degrees (2 or 4), and/or different strengths of metal–support interaction. Work is under progress to discriminate between these factors. However, the abnormally high H_2 consumption found during TPR reduction of the Pt/KL and Pt/Csβ samples (corresponding to H/Pt = 9 and 7, respectively) implies that species other than Pt^{2+} and Pt^{4+} are reduced. These results may be understood if we take into consideration the existence of very small Pt clusters as mentioned above, which could migrate close to alkali species. These species could then be reduced by hydrogen molecules activated on these Pt clusters, contributing thus to the high H/Pt ratio. From a thermodynamic point of view, the reduction of alkali ions at 500°C is unlikely to occur. Therefore, it is proposed that, during the preparation, a part of the alkali species are stabilized as an oxidized species such as K_2O and Cs_2O. A possible effect of highly basic oxides on the surface structure

of the metal clusters was reported (23). The above interpretation is speculative and further experiments, where Cs is incorporated as an oxide, are being performed.

By contrast with the results discussed above, the H/Pt ratios close to 2, observed for the Na-containing Pt/NaCsβ samples, suggest the presence of Pt species at an oxidation degree 2^+. Moreover, the single high temperature peak at 400°C, observed for these samples in agreement with the results of Lee *et al.* (43), suggests that they correspond to bare Pt^{2+} ions.

3. Infrared Results of CO Adsorbed at 100°C

The assignment of the high (HFB) and low frequency band (LFB) on Pt/KL zeolite have been the matter of controversial interpretations. Many investigations on CO adsorption are performed at high CO coverages, thus including effects of vibrational coupling and chemical shifts (17b, 47, 48). For CO adsorbed at atmospheric pressure, the muticomponent bands have recently been proposed to arise from the formation of Pt carbonyl complexes (49).

The high frequency band was thought to result from CO adsorption on larger particles while the position of the LFB was shown to depend on the alkali ion (17b, 50). Therefore, the shift to lower frequencies has been interpreted by an increase of the electronic density of the *d* orbitals of the platinum particles, leading to increased occupation of the $2\pi^*$ orbital and subsequent weakening of the CO bond (17b, 18, 41, 51). The transfer of electrons to the metal particle was attributed to the basicity of the oxygen atoms in the vicinity of the alkali ion (17b, 18, 41, 52) . For the multicomponent LFB, Ostgard *et al.* suggested that these bands correspond to CO bonded to Pt_nH^+ clusters with various degrees of electron deficiency (15). In our case, the absence of a well-defined OH band characteristic of protons (at 3610 cm^{-1}) rules out this hypothesis.

An alternative explanation to the electronic effect of the metal–support interaction is the so-called geometric effect, where the morphology of small particles exhibit unsaturated sites (corners, kinks, edges, and faces of platinum particles) with modified electronic structure. Blyholder's model indicates that the more unsaturated the site, the lower the CO frequency (53). The overlapped components below 2000 cm^{-1} represent different unsaturated sites of platinum particles (17b, 54, 55). Thus, a linear decrease of the position of the CO band with decreasing number of coordination was found (54, 55).

Recently Lane *et al.* (56), in a comparative study on K-containing supports (zeolites and silica), attributed the HFB and LFB of the Pt/KL sample to CO adsorbed on Pt located in different environments. The LFB was attributed to the electrostatic interaction of the oxygen atom of the CO molecule with the potassium cation ($Pt\text{-}CO\cdots K^+$), whereas the HFB corresponded to unpertubed CO (Pt-CO). This interpretation was supported by Kappers *et al.* (47), who showed that adsorption of water on the K^+ ion screened this effect and led to higher CO frequencies. Moreover, the broadness of the multicomponent bands was mainly explained by the distribution of the platinum size particles (57).

The effect of water on the spectra of CO adsorbed on Pt/KL was recently reinvestigated by Menacherry and Haller (58a). In contrast to the experimental conditions of Kappers *et al.* (57), their working conditions corresponded to a redistribution of the population of the CO oscillators and to decreased dipole–dipole interactions. These authors find a redshift of the CO frequency with increasing uptake of water and completely disagree with the attribution of the LFB to the interaction of CO with K^+ cation.

The effect of the alkali promoters on the frequency of CO has extensively been studied from a theoretical point of view (59). The downward shift is explained by the transfer of the alkali electrons to the $2\pi^*$ antibonding CO orbitals. With alkali cations acting as Lewis acids, a direct electrostatic interaction is considered as for organometallic salts (60). Experimental results of the CO shifts, when alkali ions are present, indicate low CO frequencies in the 1700–1800 cm^{-1} (61, 62). In our opinion, the position of the LBF observed on Pt/KL around 1930 cm^{-1} is too high and thus cannot be assigned to a direct electrostatic $CO\text{–}K^+$ interaction. However, the study of Lane *et al.* (56) obviously shows the influence of the K^+ ion. The effect of the alkali cation may rather be attributed to the increased basicity of the oxygen atoms close to the alkali cation and to the platinum particle, leading to decreased CO frequency.

Turning now to our samples, the Na-containing samples show a single band in the 2073–2000 cm^{-1} range (HFB) for CO adsorption at 100°C, while the Pt/Csβ and Pt/KL samples show a broad band composed of two multiplets at lower frequencies (Fig. 7B). Considering the channel-structure of these zeolites in comparison with conventional supports, it seems difficult to discard the metal–support interaction as one of the main factors leading to a shift of the CO frequencies. Although the basicity of the Pt/Csβ compound calculated from the average oxygen charge of the zeolite framework (Table 1) appears negligible, as compared to that of Pt/KL or Pt/CsX, the basic character of the β zeolites has already been shown (6, 9, 10), and thus, other factors may contribute to this basicity (6, 7).

CONCLUSION

The infuence of Cs on Pt/NaCsβ zeolites was investigated in the *n*-hexane transformation. The efficiency of these systems was compared to that of the Pt/KL zeolite. A set of catalysts with different Na/Cs ratios was prepared and Pt was introduced by exchange from the Pt tetraammine precursor. The reduced catalysts were mainly characterized by TPR, TEM, and FTIR of CO probe molecules. The catalytic

results, as well as the TPR and IR results (existence of a low CO frequency band), pointed out the peculiar behavior of the 100% Cs-exchanged beta and of the Pt/KL samples. A significant increase in the selectivity to aromatization to benzene was found, in comparison to the Na-containing samples. Platinum particles embedded in the zeolite lattice with a mean size of 17 Å were observed for the Pt/Csβ and Pt/KL samples while the Pt/Naβ exhibited some large particles at the external surface of the zeolite ($d = 21$ Å). The enhanced selectivity to aromatization and the correlative decrease in deactivation was explained, assuming the presence of very small Pt clusters which could not be detected by TEM. This hypothesis is strengthened by the TPR results which show a high H/Pt ratio for these two samples (H/Pt > 7) suggesting the reduction of part of alkali species (as oxides) in the proximity with small Pt clusters where hydrogen is activated.

Controversial interpretations are reported to account for the LFB observed in the presence of K^+ ions in Pt/KL. First, the electronic effect through the metal–support interaction. Then, a geometric effect related to the morphology of small particles, inducing a modification of the electronic structure of unsaturated surface Pt atoms. These two hypotheses have often been chosen one at the exclusion of the other. A third model corresponds to the direct effect of alkali metals or the electrostatic interaction of the K^+ ion with CO. Indeed, all these factors contribute to lower the CO frequency. Thus, it seems not possible to discard the metal–support interaction as in previous studies (54). In our samples, the experimental position of the LFB (1990 cm^{-1}) seems too high to account for an electrostatic interaction of the K^+ ion with the CO dipole, and therefore, the metal–support interaction has to be considered. The existence of alkali ions in the proximity of small Pt clusters would increase the basicity of neighbouring oxygen atoms of the support and favour an electron transfer to the metal particle. Our interpretation is in line with the recent work of Menacherry and Haller (58b).

For the Na-containing samples the selectivity results could suggest that Pt particles ignore the Cs^+ ions and are near the Na^+ ions. In fact, the IR results show that Pt particles are neither in close contact with Na^+ nor with Cs^+ ions up to a 75% exchange into Cs. The whole results suggest that only very small Pt clusters generated in a Pt/Csβ (Pt/KL) sample can migrate in the zeolites channels and be stabilized near the Cs^+ (K^+) ions. In this case, the efficiency in aromatization properties increases and the basicity of these ions increases the metal particle electron density.

ACKNOWLEDGMENTS

The authors gratefully acknowledge the European Commission for financial support under HCM Contract, Award ERBCHRXCT 940477. We thank M. Lavergne for the TEM work and J. Lehman for assistance for the TPR experiments. We warmly thank Drs. C. Naccache and P. Meriaudeau for helpfull discussions.

REFERENCES

1a. Hoefnagel, A. J., and van Bekkum, H., *Appl. Catal. A: General* **97**, 87 (1993).
1b. Rigutto, M. S., de Vries, H. J. A., Magill, S. R., Hoefnagel, A. J., and van Bekkum, H., *Stud. Surf. Sci. Catal.* **78**, 661 (1993).
2. Smith, K., Musson, A., and DeBoos, G. A., *J. Chem. Soc., Chem. Commun.*, 469 (1996).
3. Bellussi, G., Pazzuconi, G., Perego, C., Girotti, G., and Terzoni, G., *J. Catal.* **157**, 227 (1995).
4. Jansen, J. C., Creyghton, E. J., Lan Njo, S. L., van Koningsveld, H., and van Bekkum, H., *Catal. Today* **38**, 205 (1997).
5a. Newsam, J. M., Treacy, M. M. J., Koetsier, W. T., and de Gruyter, C. B., *Proc. Roy. Soc. A* **420**, 375 (1988).
5b. Higgins, J. B., LaPierre, R. B., Schenker, J. L., Rohrman, A. C., Wood, J. D., Kerr, G. T., and Rohrbaugh, W. J., *Zeolites* **8**, 446 (1988).
6. Camblor, M. A., Corma, A., Martin-Aranda, R. M., and Perez-Pariente, J., *in* "Proc. 9th Int. Zeol. Conf., Montreal" (R. Von Baallmoos, J. B. Higgins, and M. M. J. Treacy, Eds.), Vol II, p. 647. Butterworth-Heinemann Boston, 1993.
7. Papai, I., Goursot, A., and Fajula, F., *J. Phys. Chem.* **98**, 4654 (1994).
8. Sanderson, R. T., *in* "Chemical Bonds and Bond Energy." Academic Press, New York, 1976.
9. Dzwigaj, S., de Mallmann, A., and Barthomeuf, D., *J. Chem. Soc., Faraday Trans I* **86**, 431 (1990).
10. Barthomeuf, D., *Catal. Rev.* **38**, 521 (1996).
11. Bernard, J. R., *in* "Proc. 9th Int. Zeol. Conf., Naples" (L. V. C. Rees, Ed.), p. 686. Heyden, London, 1980.
12. Hugues, T. R., Buss, W. C., Tamm, P. W., and Jacobson, R. L., *Stud. Surf. Sci. Catal.* **28**, 725 (1986).
13a. Hong, S. B., Mielczarski, E., and Davis, M. E., *J. Catal.* **134**, 349 (1992).
13b. Mielczarski, E., Hong, S. B., Davis, R. J., and Davis, M. E., *J. Catal.* **134**, 359 (1992).
14. Larsen, G., and Haller, G. L., *Catal. Today* **15**, 431 (1992).
15. Ostgard, D. J., Kustov, L., Poeppelmeier, K. R., and Sachtler, W. M. H., *J. Catal.* **133**, 342 (1992).
16. Dossi, C., Psaro, R., Bartsch, A., Fusi, A., Sordelli, L., Ugo, R., Bellatreccia, M., Zanoni, R., and Vlaic, G., *J. Catal.* **145**, 377 (1994).
17a. Besoukhanova, C., Breysse, M., Bernard, J. R., and Barthomeuf, D., *Stud. Surf. Sci. Catal.* **6**, 201 (1980).
17b. Besoukhanova, C., Guidot, J., Barthomeuf, D., Breysse, M., and Bernard, J. R., *J. Chem. Soc., Faraday Trans I* **77**, 1595 (1981).
18a. Larsen, G., and Haller, G. L., *Catal. Lett.* **3**, 103 (1989).
18b. Dong, J. L., Zhu, J. H., and Xu, Q. H., *Appl. Catal. A: General* **112**, 105 (1994).
19a. Tauster, S. J., and Steger, J. J., *Mater. Res. Soc. Symp. Proc.* **111**, 419 (1988).
19b. Tauster, S. J., and Steger, J. J., *J. Catal.* **125**, 387 (1990).
20a. Lane, G. S., Modica, F. S., and Miller, J. T., *J. Catal.* **129**, 145 (1991).
20b. Gao, Z., Jiang, X., Ruan, Z., and Xu, Y., *Catal. Lett.* **19**, 81 (1993).
21. Derouane, E. G., and Vanderveken, D. J., *Appl. Catal.* **45**, L15 (1988).
22a. Davis, R. J., and Derouane, E. G., *Nature* **349**, 313 (1991).
22b. Davis, R. J., and Derouane, E. G., *J. Catal.* **132**, 269 (1991).
23. Davis, R. J., *HCR* **1**, 41 (1994).
24. Meriaudeau, P., and Naccache, C., *Catal. Rev. Sci. Eng.* **39**, 5 (1997).
25. Smirniotis, P. G., and Ruckenstein, *Appl. Catal. A: General* **123**, 59 (1995).
26a. Zheng, J., Dong, J. L., and Xu, Q. H., *Stud. Surf. Sci. Catal.* **84**, 1641 (1994),
26b. Zheng, J., Dong, J. L., Xu, Q. H., Liu, Y., and Yan, A. Z., *Appl. Catal.* **126**, 141 (1995).
27. Maldonado, F. J., *et al.* to be published.
28. Perez-Pariente, J., Martens, J. A., and Jacobs, P. A., *Appl. Catal.* **31**, 35 (1987).

29a. Léglise, J., Manoli, J. M., Potvin, C., Djéga-Mariadassou, G., and Cornet, D., *J. Catal.* **152**, 275 (1995).
29b. Klug, H. P., and Alexander, L. E., *in* "X-Ray Diffraction Procedures." Wiley, New York, 1954.
30. Bourgeat-Lami, E., Fajula, F., Anglerot, D., and Des Courières, T., *Micro. Mater.* **1**, 237 (1993).
31. Breck, D. W., *in* "Zeolite Molecular Sieves: Structure, Chemistry and Use," p. 432. Wiley, New York, 1974.
32. Zheng, J., Dong, J., Xu, Q., and Hu, C., *Catal. Lett.* **37**, 25 (1996).
33. Sheppard, N. J., and Nguyen, T. T., *Adv. Infrared Raman Spectrosc.* **5**, 67 (1978).
34a. McHugh, B. J., Larsen, G., and Haller, G. L., *J. Phys. Chem.* **94**, 8261 (1990).
34b. Larsen, G., and Haller, G. L., *Catal. Lett.* **17**, 127 (1993).
35. Iglesia, E., and Baumgartner, *Stud. Surf. Sci. Catal.* **75**, 993 (1993).
36. Kao, J. L., Mc Vicker, G. B., Treacy, M. M. J., Rice, S. B., Robbins, J. L., Gates, W. E., Ziemiak, J. J., Cross, V. R., and Vanderspurt, T. H., *Stud. Surf. Sci. Catal.* **75**, 1019 (1993).
37. Vaarkamp, M., Miller, J. T., Modica, F. S., Lane, G. S., and Koningsberger, D. C., *J. Catal.* **138**, 675 (1992).
38. Barthomeuf, D., and de Mallmann, A., *Stud. Surf. Sci. Catal.* **37**, 365 (1988).
39. Vaarkamp, M., Grondelle, J. V., Miller, J. T., Sajkowski, D. J., Modica, F. S., Lane, G. S., Gates, B. C., and Koningsberger, D. C., *Catal. Lett.* **6**, 369 (1990).
40. Han, W. J., Kooh, A. B., and Hicks, R. F., *Catal. Lett.* **18**, 193 (1993).
41. Bernard, J. R., and Breysse, M., private communication.
42a. Chmelka, B. F., Rosin, R. R., Went, G. T., Bell, A. T., Radke, C. J., and Petersen, E. E., *Stud. Surf. Sci. Catal.* **49**, 995 (1989).
42b. Park, S. H., Tzou, M. S., and Sachtler, W. M. H., *Appl. Catal.* **24**, 85 (1986).
42c. Creyghton, E. J., van Duin, A. C. T., Jansen, J. C., Kooyman, P. J., Zandbergen, H. W., and van Bekkum, H., *J. Chem. Soc., Faraday Trans.* **92**, 4637 (1996).
43. Lee, J. K., and Rhee, H. K., *Catal. Today* **38**, 235 (1997).
44. Sachtler, W. M. H., and Zhang, Z., *Adv. Catal.* **39**, 129 (1993).
45. Chae, J. H., and Moon, S. H., *Stud. Surf. Sci. Catal.* **105**, 877 (1997).
46. Vaarkamp, M., van Grondelle, J., van Santen, R. A., Miller, J. T., Meyers, B. L., Modica, F. S., Lane, G. S., and Koningsberger, D. C., *in* "Proc. 9th Int. Zeol. Conf., Montreal" (R. Von Baallmoos, J. B. Higgins, and M. M. J. Treacy, Eds.), Vol. II, p. 433. Butterworth–Heinemann, Boston, 1993.
47. Kappers, M. J., Vaarkamp, M., Miller, J. T., Modica, F. S., Barr, M. K., van der Maas, J. H., and Koningsberger, D. C., *Catal. Lett.* **21**, 235 (1993).
48. Kustov, L. M., Ostgard, D., and Sachtler, W. M. H., *Catal. Lett.* **9**, 121 (1991).
49. Stakheev, A. Y., Shpiro, E. S., Jaeger, N. I., and Schulz-Ekloff, G., *Catal. Lett.* **34**, 293 (1995).
50. Stakheev, A. Y., Shpiro, E. S., Jaeger, N. I., and Schulz-Ekloff, G., *Catal. Lett.* **32**, 147 (1995).
51a. Dai, L. X., Sakashita, H., and Tatsumi, T., *Bull. Chem. Soc. Jpn* **67**, 1553 (1994).
51b. Dai, L. X., Sakashita, H., and Tatsumi, T., *J. Catal.* **147**, 311 (1994).
52. de Mallmann, A., and Barthomeuf, D., *Stud. Surf. Sci. Catal.* **46**, 429 (1989).
53. Blyholder, G., *J. Phys. Chem.* **68**, 2772 (1964).
54. Kappers, M. J., and Van der Maas, J. H., *Catal. Lett.* **10**, 365 (1991).
55. Brandt, R. K., Hughes, M. R., Bourget, L. P., Truszkowska, K., and Greenler, R. G., *Surf. Sci.* **286**, 15 (1993).
56. Lane, G. S., Miller, J. T., Modica, F. S., and Barr, M. K., *J. Catal.* **141**, 465 (1992).
57. Kappers, M. J., Miller, J. T., and Koningsberger, D. C., *J. Phys. Chem.* **100**, 3227 (1996).
58a. Menacherry, P. V., and Haller, G. L., *Catal. Lett.* **44**, 135 (1997).
58b. Menacherry, P. V., and Haller, G. L., *J. Catal.* **177**, 175 (1998).
59a. Holloway, S., Norskov, J. K., and Lang, N. D., *J. Chem. Soc., Faraday Trans I* **83**, 1935 (1987).
59b. van Santen, R. A., *J. Chem. Soc., Faraday Trans I* **83**, 1915 (1987).
60. Darensbourg, M. Y., *Prog. Inorg. Chem.* **33**, 221 (1984).
61a. Angevaare, P. A. J. M., Hendrickx, H. A. C. M., and Ponec, V., *J. Catal.* **110**, 11 (1988).
61b. Angevaare, P. A. J. M., Hendrickx, H. A. C. M., and Ponec, V., *J. Catal.* **110**, 18 (1988).
62. Pitchon, V., Primet, M., and Praliaud, H., *Appl. Catal.* **62**, 317 (1990).
63. Maldonado-Hodar, F. J., Ribeiro, M. F., Silva, J. M., Antunes, A. P., and Ribeiro, F. R., *J. Catal.* **178**, 1 (1998).